arXiv:1401.3414v1 [cond-mat.str-el] 15 Jan 2014

Suppression of antiferromagnetic order and hybridization gap by electron- and hole-doping in the Kondo semiconductor $CeOs_2Al_{10}$

J. Kawabata,[1] T. Takabatake,[1,2,*] K. Umeo,[3,1,†] and Y. Muro[4]

[1]*Department of Quantum matter, AdSM, Hiroshima University, Higashi-Hiroshima 739-8530, Japan*

[2]*Institute for Advanced Materials Research, Hiroshima University, Higashi-Hiroshima 739-8530, Japan*

[3]*Cryogenics and Instrumental Analysis Division, N-BARD, Hiroshima University, Higashi-Hiroshima 739-8526, Japan*

[4]*Liberal Arts and Sciences, Faculty of Engineering, Toyama Prefectural University, Izumi 939-0398, Japan*

(Dated: January 16, 2014)

Abstract

The Kondo semiconductor $CeOs_2Al_{10}$ exhibits an antiferromagnetic (AFM) order at $T_N = 28.5$ K, whose temperature is unexpectedly high for the small ordered moment of 0.3 μ_B/Ce. We have studied the effects of electron- and hole-doping on the hybridization gap and AFM order by measuring the magnetization M, magnetic susceptibility χ, electrical resistivity ρ, and specific heat C on single crystals of $Ce(Os_{1-x}Ir_x)_2Al_{10}(x \leq 0.15)$ and $Ce(Os_{1-y}Re_y)_2Al_{10}(y \leq 0.1)$. The results of $M(B)$ indicates that the AFM ordered moment μ_{AF} changes the direction from the c-axis for $x = 0$ to the a-axis for $x = 0.03$. With increasing x up to 0.15, T_N gradually decreases although the $4f$ electron state becomes localized and the magnitude of μ_{AF} is increased to 1 μ_B/Ce. With increasing y, the $4f$ electron state is more delocalized and the AFM order disappears at a small doping level $y = 0.05$. In both electron- and hole-doped systems, the suppression of T_N is well correlated with the increase of the Sommerfeld coefficient γ in $C(T)$. Furthermore, the simultaneous suppression of T_N and the semiconducting gap in $\rho(T)$ at $T > T_N$ indicates that the presence of the hybridization gap is indispensable for the unusual AFM order in $CeOs_2Al_{10}$.

I. INTRODUCTION

In a few cerium-based compounds, hybridization of $4f$ electrons and conduction bands (c-f hybridization) gives rise to a hybridization gap in the vicinity of the Fermi level.[1] Because of the strong electron correlation, the energy gap is renormalized to a small value of 10-100 K. So-called Kondo semiconductors such as $Ce_3Bi_4Pt_3$ and CeRhAs display semiconducting behavior in the electrical resistivity,[2,3] while so-called Kondo semimetals CeNiSn and CeRhSb show semimetallic behavior.[3,4] The latter behavior reflects the anisotropic gap which closes in a particular direction due to the anisotropy of the hybridization.[5–7] These compounds belong to the valence fluctuating regime and do not order magnetically at low temperatures because the strong Kondo interaction between the $4f$ localized moment and conduction electron spins screens the localized moments. However, doping of $3d$ electrons in CeNiSn by Cu substitution for Ni at a several % level induces a long-range antiferromagnetic (AFM) order.[8,9] The emergence of AFM order was attributed to the weakened c-f exchange interaction which is a consequence of the increase of the Fermi level with respect to the $4f$ level. On the other hand, doping of $3d$ holes in CeNiSn by Co substitution for Ni strengthens the c-f exchange interaction and thus increases the Kondo temperature T_K.[9–11]

A family of compounds CeT_2Al_{10}(T = Fe, Ru, Os) with the orthorhombic $YbFe_2Al_{10}$-type structure display semiconducting behavior in the resistivity at high temperatures and thus they were classified into Kondo semiconductors.[12–14] The Fe compound, where the c-f hybridization is strongest among the three, belongs to the valence fluctuation regime and thus the ground state remains in a paramagnetic state.[12] However, the isoelectronic compounds with T = Ru and T = Os order antiferromagnetically at rather high Néel temperature T_N of 27 K and 28.5 K, respectively.[13–21] It evoked a question why the T_N's of the Ce compounds with small magnetic moments $0.3 - 0.4$ μ_B/Ce are higher than those of Gd counterparts with 7 μ_B/Gd.[16,17] The ordering temperatures may be scaled by the de Gennes factor as long as the magnetic order is caused by the Ruderman – Kittel – Kasuya – Yosida (RKKY) interaction.[22] According to the de Gennes scaling, T_N for a Ce compound is expected to be 1/100 of that for the Gd counterpart if we neglect the crystal field effect and possible difference in the Fermi surface. Optical conductivity measurements for CeT_2Al_{10}(T = Ru, Os) have revealed the CDW-like instability which develops along the b axis at temperatures slightly higher than T_N. It was suggested that this electronic instability

induces the AFM order.[23] Another enigma is why the ordered moments $\mu_{\rm AF}$ point along the c axis although the magnetic susceptibility is largest for $B \parallel a$; $\chi(B \parallel a) \gg \chi(B \parallel c) > \chi(B \parallel b)$.[17–21]

As mentioned above, previous studies of the Kondo semimetal CeNiSn by doping $3d$ electrons and holes provided us with important information on the relation between the hybridization gap and magnetism. For better understanding of the unusual magnetic order in $CeOs_2Al_{10}$, we have conducted a systematic study by substituting Ir and Re for Os, which dope $5d$ electrons and $5d$ holes, respectively. A part of the experimental results on the Ir substituted samples has been reported in a proceeding of a conference.[24]

II. PREPARATION AND CHARACTERIZATION OF SINGLE CRYSTALS

Homogeneity ranges in $Ce(Os_{1-x}Ir_x)_2Al_{10}$ and $Ce(Os_{1-y}Re_y)_2Al_{10}$ were examined by preparing polycrystalline samples with the nominal compositions of Ir and Re up to 50%. The arc melted samples were annealed in an evacuated quartz ampoule at 850 °C for 7 days. The samples were characterized by combining metallographic examination, powder x-ray diffraction, and wavelength dispersive electron-probe microanalysis (EPMA). The Re-substituted samples were found to be homogeneous with the composition close to the initial one. However, the bottom part of the Ir substituted sample contains an Ir rich phase of $CeOsIr_3Al_{15}$ and the Ir composition in the upper part is smaller than the initial one. With the initial composition of $X = 0.5$, for example, the real composition x was 0.38. We note that the presence of the compound $CeIr_2Al_{10}$ was not reported but there is a report on $CeRe_2Al_{10}$ with a distinct structure from that of $CeOs_2Al_{10}$.[25] X-ray diffraction analysis showed that the $YbFe_2Al_{10}$-type structure is kept in the whole ranges $x \leq 0.4$ and $y \leq 0.5$. The lattice parameters are plotted in Fig. 1. Because the change is smaller than 0.3% for $x \leq 0.2$ and $y \leq 0.1$, we expect that the chemical pressure effect on the c-f hybridization may be much weaker than that of doping of $5d$ electrons and holes in the above composition range.

Single crystalline samples were grown using an Al self-flux method as reported previously.[15] Alloys of $Ce(Os_{1-X}Ir_X)_2$ and $Ce(Os_{1-Y}Re_Y)_2$ were prepared by arc melting of pure elements. The crushed alloy ingots together with an excess amount of Al in the composition of 1 : 2 : 30 were loaded into an aluminum crucible, which was sealed in a quartz ampoule under an Ar

atmosphere of 1/3 atm. The ampoule was heated to 1200 °C, kept for 5 hours, and slowly cooled at a ratio 2 °C/h to 720 °C, at which temperature the molten Al flux was separated by centrifuging. Several crystals of approximately $2 \times 2 \times 3$ mm^3 were obtained. The atomic composition was determined by EPMA. The real compositions of Ir (x) were found to be 0, 0.03, 0.04, 0.08, and 0.15 for the initial ones $X = 0, 0.02, 0.03, 0.10$, and 0.20, respectively, while the compositions of Re (y) were same as the initial ones $Y = 0.01, 0.02, 0.03, 0.05$, and 0.1. The difference between the values of x and X is attributed to the segregation of a small amount of impurity phase of (Os, Ir)Al_4. For the measurements of physical properties, we carefully avoided the parts containing impurity phases. After the single-crystal nature was verified by the Laue back diffraction method, the crystals were cut in an appropriate shape for the measurements.

III. MAGNETIC, TRANSPORT, AND THERMAL PROPERTIES

A. Magnetic susceptibility and magnetization

Using single crystalline samples mentioned above, we have studied the magnetic, transport, and thermal properties. The measurement of magnetic susceptibility $\chi(T)$ was performed in an external field $B = 1$ T from 1.8 K to 300 K with a Quantum Design Magnetic Property Measurements System (MPMS). The isothermal magnetization $M(B)$ was measured up to $B = 14$ T by the dc extraction method using a Quantum Design Physical Property Measurement System (PPMS). An ac four-probe method was used for the electrical resistivity $\rho(T)$ measurements from 2.6 K to 300 K. The specific heat $C(T)$ was measured from 2 K to 300 K by the relaxation method in PPMS.

Figures 2(a) and 2(b) display, respectively, the variations of $\chi(T)$ for $Ce(Os_{1-x}Ir_x)_2Al_{10}(x \leq 0.15)$ and $Ce(Os_{1-y}Re_y)_2Al_{10}(y \leq 0.1)$ along the three principal axes. For the undoped sample, $\chi_a(T)$ in $B \parallel a$ passes through a maximum at around 45 K and drops at $T_N = 28.5$ K. On going from $x = 0$ to 0.15, the broad maximum changes to a sharp peak, whose temperature decreases to 7 K. Thereby, the value at the maximum increases by 5 times, leading to the enhancement of anisotropy, $\chi_a \gg \chi_c > \chi_b$. It is worth noting that the data set of $\chi_i(T)(i = a, b, c)$ for $x = 0.15$ at $T > 30$ K are in agreement with the calculation taking account of the crystal field effect on the localized $4f$ state of Ce^{3+} ion.[26,27] The solid

lines for $x = 0.15$ in Fig. 2(a) represent the calculations.[27] The observed localization of the $4f$ electron state is a consequence of the increase in the Fermi level by electron doping, as found in Cu doping in CeNiSn.[8,10] The inverse of $\chi_a(T)$ is plotted versus T in the inset. The Curie-Weiss fit to the data between 200 and 300 K gives the paramagnetic Curie temperature $\theta_{\rm p}$ which value changes from -20 K for $x = 0$ to $+26$ K for $x = 0.15$. For $B \parallel b$ and $B \parallel c$, the decrease in $\chi(T)$ at $T < T_{\rm N}$ disappears with increasing x. For $x \geq 0.08$, the sharp peak in $\chi_a(T)$ at $T_{\rm N}$ and the absence of the drop in $\chi_b(T)$ and $\chi_c(T)$ at $T < T_{\rm N}$ suggest the AFM ordered moments $\mu_{\rm AF}$ oriented parallel to the easy a axis. This reorientation of $\mu_{\rm AF}$ from $\parallel$ c-axis to $\parallel$ a-axis is confirmed by the isothermal magnetization and neutron diffraction measurements, as will be presented below.

Compared with the tendency of localization of $4f$ electrons in $Ce(Os_{1-x}Ir_x)_2Al_{10}$, an opposite trend was observed for $Ce(Os_{1-y}Re_y)_2Al_{10}$. As shown in Fig. 2(b), the maximum in $\chi_a(T)$ at around 45 K is suppressed with increasing y and the anomaly at $T_{\rm N}$ disappears at $y = 0.05$. The anomalies in $\chi_b(T)$ and $\chi_c(T)$ disappear at $y = 0.01$ and $y = 0.03$, respectively. The continuous increase in $\chi_a(T)$ on cooling to 2 K may be the effect of disorder-induced magnetic moments, which needs to be studied by microscopic experiments. The inset of Fig. 2(b) displays the inverse of $\chi_a(T)$ against T. The increase of $|\theta_{\rm p}|$ from 20 K for $y = 0$ to 46 K for $y = 0.1$ suggests the increase of $T_{\rm K}$ because the value of $T_{\rm K}$ for the overall crystal-field levels is in proportion to $|\theta_{\rm p}|$.[28]

In the undoped sample, $\mu_{\rm AF}$ is oriented along the c-axis.[20,21] When external magnetic field was applied along the c-axis at 0.3 K, a spin flop transition was observed at 6 T.[15] This transition in $M(B \parallel c)$ is found at $B_{sf} = 6.1$ T by the present measurement at 2 K as shown at the bottom of Fig. 3(a). For $x = 0.03$, however, there is no transition in $M(B \parallel c)$ but a weak upturn appears in $M(B \parallel a)$ at around 3 T. For $x = 0.08$, a metamagnetic transition in $M(B \parallel a)$ is clearly seen at 3 T. Passing through a bend at $B_s = 10.4$ T, $M(B \parallel a)$ is saturated to a large value of 0.7 $\mu_{\rm B}$/Ce. We interpret the metamagnetic transition along the easy a-axis as a spin-flop transition from $\mu_{\rm AF} \parallel a$ to $\mu_{\rm AF} \perp a$ because the linear extrapolation of the $M(B \parallel a)$ data between 8 T and 4 T goes to the origin. For $x = 0.15$, the magnitude of $M(B \parallel a)$ increases further and that of B_s decreases, but the spin-flop transition field B_{sf} does not change. These observations suggest that the ground state for $x \geq 0.08$ is the AFM state with $\mu_{\rm AF}$ ($\sim 1\mu_{\rm B}$/Ce) pointing along the a-axis. Figure 3(b) shows the results of $M(B \parallel a)$ and $M(B \parallel c)$ for the Re substituted samples. With increasing y, the

metamagnetic behavior in $M(B \parallel c)$ is barely observed for $y = 0.03$. It is not seen for $y = 0.05$, in agreement with the absence of anomaly in $\chi_a(T)$ in Fig. 2(b). The absence of anomaly in $M(B \parallel a)$ suggests that the AFM order with $\mu_{\rm AF} \parallel c$ fades away without showing reorientation.

Figure 4 shows the variations of B_{sf} and B_s as a function of x and y. As mentioned above, the AFM structure changes from $\mu_{\rm AF} \parallel c$ to $\mu_{\rm AF} \parallel a$ somewhere between $x = 0$ and $x = 0.03$. Thereby, the change in $T_{\rm N}$ is only 10% from 28.5 K to 26.5 K, suggesting that the intersite AFM interaction between Ce moments may not depend on the direction of $\mu_{\rm AF}$ with respect to the crystal axis. Recently, a neutron scattering experiment has confirmed the reorientation of ordered moments from $\mu_{\rm AF} \parallel c = 0.3$ $\mu_{\rm B}$/Ce for $x = 0$ to $\mu_{\rm AF} \parallel a = 0.9$ $\mu_{\rm B}$/Ce for $x = 0.08$.[29] Similar reorientation of AFM ordered moments has been suggested to occur in $CeRu_2Al_{10}$ when Rh is partially substituted for Ru at 5%.[30] Since both substitutions of Ir for Os and Rh for Ru dope d electrons in the mother compounds, the spin reorientation should be induced by the doping of d electrons into the gapped state. The magnitude of B_s slightly decreases but that of B_{sf} is constant in the range $0.03 \leq x \leq 0.15$. In contrast, B_{sf} is strongly suppressed by Re substitution. This result is consistent with the neutron scattering study on the sample with $y = 0.03$ which has revealed the AFM arrangement of $\mu_{\rm AF} \parallel a$ with a reduced size of 0.18 $\mu_{\rm B}$/Ce.[31] This strong suppression of $\mu_{\rm AF}$ by Re substitution indicates that even low level doping of $5d$ holes in $CeOs_2Al_{10}$ enhances the Kondo effect and prevents the system from AFM ordering.

B. Electrical resistivity

Effects of the doping on the hybridization gap above $T_{\rm N}$ and the AFM gap below $T_{\rm N}$ may manifest themselves in the temperature dependence of electrical resistivity $\rho(T)$. Figures 5(a) and 5(b) show the results of $\rho(T)$ along the three principal axes for $CeOs_2Al_{10}$ and substituted samples with Ir and Re, respectively. The vertical lines denote $T_{\rm N}$'s determined by the specific heat measurement as will be described below. The $\rho(T)$ curves for $x = 0$ strongly increase on cooling as manifested by the ratio $\rho(2.6\ {\rm K})/\rho(300\ {\rm K}) = 7$ which is higher than that of 1.6 for the previously reported data.[15] This fact indicates higher quality of the present sample. The –log$T$ dependence from 300 K to 100 K is followed by a thermal activation-type behavior in the range from 60 K to 30 K as shown in the inset. By fitting

the data with the formula $\rho = \rho_0 \exp(\Delta/2k_{\rm B}T)$, the values of $\Delta_a/k_{\rm B}$, $\Delta_b/k_{\rm B}$, and $\Delta_c/k_{\rm B}$ are estimated to be 56 K, 83 K, and 65 K, respectively, whose values are larger by 1.8 times than those reported previously.[15] The slope of $\rho(T)$ increases abruptly below $T_{\rm N} = 28.5$ K, which can be attributed to the formation of a superzone gap on the Fermi surface. Such a superzone gap is formed by folding of the Brillouin zone associated with the AFM order.[32] The semiconducting behavior at $T < 14$ K suggests opening of another gap within the hybridization gap. Successive openings of gaps at the Fermi level have been directly observed by a photoemission spectroscopic study.[33] At a small level of $x = 0.04$, the semiconducting increase at $T < 14$ K changes to a gradual decrease on cooling, although both the bend at $T_{\rm N}$ and the activation-type behavior above $T_{\rm N}$ are still observed. The magnitudes of Δ_a , Δ_b, and Δ_c for $x = 0.04$ are approximately 80% of those for $x = 0$. For $x = 0.08$, only $\rho_a(T)$ displays the bend at $T_{\rm N}$, which is consistent with the AFM arrangement of $\mu_{\rm AF} \parallel a$ along the propagation vector (1, 0, 0).[29] In addition, a hump manifests itself in $\rho_c(T)$ at around 200 K. The –log$T$ behavior above the hump can be attributed to the Kondo scattering in the crystal-field excited state.[34] For $x = 0.15$, the hump at around 200 K becomes more evident in $\rho_c(T)$ and $\rho_a(T)$, but the anomaly at $T_{\rm N}$ becomes unclear.

Let us turn our attention to the results of $\rho(T)$ for the Re substituted samples in Fig. 5(b). Even at a small level $y = 0.01$, the semiconducting behavior in $\rho(T)$ at $T < 10$ K disappears although the thermal activation behavior above $T_{\rm N}$ still exists. On going from $y = 0.01$ to $y = 0.05$, the metallic behavior at low temperatures becomes more evident. The anomaly at $T_{\rm N}$ is observed in $\rho_b(T)$ for $y = 0.02$ but is hardly observed for $y = 0.03$. For $y = 0.05$, the maximum shifts to high temperature and $\rho(T)$ at $T < 15$ K is in proportion to T^2. For $y = 0.1$, the temperature at the maximum further increases, suggesting the enhancement of $T_{\rm K}$. It is noteworthy that the thermal activation behavior above $T_{\rm N}$ disappears simultaneously with the metalization below $T_{\rm N}$. This transformation by $5d$ hole doping occurs at a lower doping level than by $5d$ electron doping.

C. Specific heat

The data of specific heat divided by temperature C/T are plotted against T in Figs. 6(a) and 6(b). The midpoint of the jump in C/T was taken as $T_{\rm N}$. For the undoped sample, C/T jumps at $T_{\rm N}$ and the extrapolation of the plot of C/T vs T^2 to $T = 0$ gives Sommerfeld

coefficient γ of 0.007 J/K^{2}mol. When x is increased to 0.04 and 0.08, $T_{\rm N}$ decreases and the jump becomes smaller. For $x = 0.15$, C/T gradually increases on cooling from 17 K and exhibits a jump at 7 K, which temperature agrees with that of the sharp peak in $\chi_a(T)$ in Fig. 2(a). As is shown in Fig. 6(b), with increasing y, the jump at $T_{\rm N}$ gradually decreases and disappears at $y = 0.05$. The γ value increases to 0.1 J/K^{2}mol at $y = 0.1$.

The values of $T_{\rm N}$ and γ are plotted as a function of x and y in Fig. 7(a). As $5d$ electrons or holes are doped, the value of $T_{\rm N}$ is suppressed and the γ value is increased. The opposite change in $T_{\rm N}$ and γ indicates that the development of the density of the states at the Fermi level destroys the AFM order. This fact seems to be inconsistent with the AFM order caused by the RKKY mechanism, in which the magnetic interaction between neighboring Ce moments is mediated by the spin polarization of conduction electrons at the Fermi level. When the conduction electron density is increased, the spin polarization would be enhanced, leading to the increase of $T_{\rm N}$. Another interesting observation in Fig. 7(a) is the fact that both the suppression of $T_{\rm N}$ and increase of γ value are more drastic as a function y than as a function of x. When $5d$ holes are doped, the Fermi level is lowered toward the $4f$ electron level. Then, the c-f exchange interaction will be strengthened and the valence fluctuation will be enhanced, as found in the case of Co substitution for Ni in CeNiSn.[10,11] Another method to enhance the c-f exchange interaction in Ce based compounds is the application of pressure. A previous study of $CeOs_2Al_{10}$ under pressure showed that $T_{\rm N}$ is almost constant up to $P = 2.3$ GPa and suddenly suppressed as the pressure is further increased.[35] It is noteworthy that the suppression of $T_{\rm N}$ by pressure coincides with the metallization in $\rho(T)$ at $T < T_{\rm N}$, which resembles the observation in the present experiment by doping $5d$ holes.

Finally, we focus on the relation between the hybridization gap and the AFM order. Figure 7(b) shows the variations of $T_{\rm N}$ and thermal activation energy Δ in the resistivity as a function of x and y. We find strong correlation between the variations of $T_{\rm N}$ and Δ. This correlation indicates that the presence of the hybridization gap is indispensable for the AFM order at unusually high $T_{\rm N}$. In order to prove this idea, we plan to do photoemission and electron-tunneling experiments which can probe the temperature dependence of the hybridization gap in Kondo semiconductors.[36,37]

IV. SUMMARY

We studied the effects of doping of $5d$ electrons and holes on the Kondo semiconductor $CeOs_2Al_{10}$ by measuring $\chi(T)$, $M(B)$, $\rho(T)$, and $C(T)$ on single crystalline samples of $Ce(Os_{1-x}Ir_x)_2Al_{10}(x \leq 0.15)$ and $Ce(Os_{1-y}Re_y)_2Al_{10}(y \leq 0.1)$. The valence fluctuation behavior in $\chi_a(T)$ with a broad maximum at around 45 K for the undoped sample changes to the Curie-Weiss behavior of Ce^{3+} with increasing x. This change means that doping of $5d$ electrons localizes the $4f$ electron state in $CeOs_2Al_{10}$. With increasing y, on the contrary, the broad maximum of $\chi_a(T)$ decreased and disappeared. The spin-flop transition in $M(B)$ for the Ir substituted samples revealed that the direction of the ordered moment μ_{AF} changes from $\parallel$ c-axis to $\parallel$ a-axis with increasing x to 0.03. In spite of the significant increase of μ_{AF} from 0.3 μ_B/Ce for $x = 0$ to 1 μ_B/Ce for $x = 0.15$, T_N decreases gradually from 28.5 K to 7.0 K. By the Re substitution, T_N disappears at a small level $y = 0.05$. The results of $\rho(T)$ and $C(T)$ showed that the development of density of states at the Fermi level causes metallization at $x \cong 0.08$ and $y \cong 0.02$, respectively. Furthermore, the suppression of T_N is well correlated with that of gap energy Δ as a function of x and y. Therefore, we conclude that the presence of the hybridization gap is indispensable for the AFM order at unusually high T_N in $CeOs_2Al_{10}$.

ACKNOWLEDGMENTS

We thank K. Yutani and Y. Yamada for their help in the preparation of samples. We acknowledge valuable discussions with T. Onimaru, D. T. Adroja, and T. Yokoya. This work was supported by a Grant-in-Aid of MEXT, Japan (Grant No. 20102004 and 23840033).

---

* takaba@hiroshima-u.ac.jp

† kumeo@sci.hiroshima-u.ac.jp

[1] For a review, see P. S. Riseborough, Adv. Phys. **49**, 257 (2000).

[2] M. F. Hundley, P. C. Canfield, J. D. Thompson, Z. Fisk, and J. M. Lawrence, Phys. Rev. B **42**, 6842 (1990).

[3] T. Takabatake, T. Sasakawa, J. Kitagawa, T. Suemitsu, Y. Echizen, K. Umeo, M. Sera, and Y. Bando, Physica B **328**, 53 (2003).

[4] T. Takabatake, F. Teshima, H. Fujii, S. Nishigori, T. Suzuki, T. Fujita, Y. Yamaguchi, J. Sakurai, and D. Jaccard, Phys. Rev. B **41**, 9607 (1990).

[5] M. Kyogaku, Y. Kitaoka, H. Nakamura, K. Asayama, T. Takabatake, F. Teshima, and H. Fujii, J. Phys. Soc. Jpn. **59**, 1728 (1990).

[6] H. Ikeda and K. Miyake, J. Phys. Soc. Jpn. **65**, 1769 (1996).

[7] J. Moreno and P. Coleman, Phys. Rev. Lett. **84**, 342 (2000).

[8] T. Takabatake, Y. Nakazawa, M. Ishikawa, T. Sakakibara, K. Koga, and I. Oguro, J. Mag. Mag. Mat. **76&77**, 97 (1988).

[9] K. Nakamura, Y. Kitaoka, K. Asayama, T. Takabatake, G. Nakamoto, H. Tanaka, and H. Fujii, Phys. Rev. B **53**, 6385 (1996).

[10] T. Takabatake, G. Nakamoto, H. Tanaka, H. Fujii, S. Nishigori, T. Suzuki, T. Fujita, M. Ishikawa, I. Oguro, M. Kuris, and A.A. Menovsky, *Transport and Thermal Properties of f-Electron Systems*, edited by G. Oomi, H. Fujii, and T. Fujita (Plenum Press, New York, 1993) p. 1.

[11] D. T. Adroja, B. D. Rainford, J. M. de Teresa, A. del Moral, M. R. Ibarra, and K. S. Knight, Phys. Rev. B **52**, 12790 (1995).

[12] Y. Muro, K. Motoya, Y. Saiga, and T. Takabatake, J. Phys. Soc. Jpn. **78**, 083707 (2009).

[13] A. M. Strydom, Physica B **404**, 2981 (2009).

[14] T. Nishioka, Y. Kawamura, T. Takesaka, R. Kobayashi, H. Kato,M. Matsumura, K. Kodama, K. Matsubayashi, and Y. Uwatoko, J. Phys. Soc. Jpn. **78**, 123705 (2009).

[15] Y. Muro, J. Kajino, K. Umeo, K. Nishimoto, R. Tamura, and T. Takabatake, Phys. Rev. B **81**, 214401 (2010).

[16] Y. Muro, J. Kajino, T. Onimaru, and T. Takabatake, J. Phys. Soc. Jpn. **80**, SA021 (2011).

[17] H. Tanida, D. Tanaka, M. Sera, C. Moriyoshi, Y. Kuroiwa, T. Takesaka, T. Nishioka, H. Kato, and M. Matsumura, J. Phys. Soc. Jpn. **79**, 083701 (2010).

[18] D. D. Khalyavin, A. D. Hillier, D. T. Adroja, A. M. Strydom, P. Manuel, L. C. Chapon, P. Peratheepan, K. Knight, P. Deen, C. Ritter, Y. Muro, and T. Takabatake, Phys. Rev. B **82**, 100405(R) (2010).

[19] S. Kambe, H. Chudo, Y. Tokunaga, T. Koyama, H. Sakai, U. Ito, K. Ninomiya, W. Higemoto, T. Takesaka, T. Nishioka, and Y. Miyake, J. Phys. Soc. Jpn. **79**, 053708 (2010).

[20] D. T. Adroja, A. D. Hillier, P. P. Deen, A. M. Strydom, Y. Muro, J. Kajino, W. A. Kockelmann, T. Takabatake, V. K. Anand, J. R. Stewart, and J. Taylor, Phys. Rev. B **82**, 104405(2010).

[21] H. Kato, R. Kobayashi, T. Takesaka, T. Nishioka, M. Matsumura, K. Kaneko, and N. Metoki, J. Phys. Soc. Jpn. **80**, 073701 (2011).

[22] K. N. R. Taylor and M. I. Darby, *Physics of Rare Earth Solids* (Chapman and Hall Ltd, London, 1970).

[23] S. Kimura, T. Iizuka, H. Miyazaki, A. Irizawa, Y. Muro, T. Takabatake, Phys. Rev. Lett. **106**, 056404 (2011).

[24] J. Kawabata, K. Yutani, K. Umeo, T. Takabatake, Y. Muro, JPS. Conf. Proc. in press.

[25] A. S. Sefat, S. L. Bud'ko, P. C. Canfield, Phys. Rev. B **79**, 174429 (2009).

[26] K. Yutani, Y. Muro, J. Kajino, T. J. Sato, and T. Takabatake, J. Phys.: Conf. Ser. **391**, 012070 (2012).

[27] F. Strigari, T. Willers, Y. Muro, K. Yutani, T. Takabatake, Z. Hu, S. Agrestini, C.-Y. Kuo, Y.-Y. Chin, H.-J. Lin, T. W. Pi, C. T. Chen, E. Weschke, E. Schierle, A. Tanaka, M. W. Haverkort, L. H. Tjeng, and A. Severing, Phys. Rev. B **87**, 125119 (2013).

[28] N. B. Brandt and V. V. Moshchalkov, Adv. Phys. **33**, 373 (1984).

[29] D. D. Khalyavin, D. T. Adroja, P. Manuel, J. Kawabata, K. Umeo, T. Takabatake, and A. M. Strydom, Phys. Rev. B **88**, 060403(R) (2013).

[30] A. Kondo, K. Kindo, K. Kunimori, H. Nohara, H. Tanida, M. Sera, R. Kobayashi, T. Nishioka, and M. Matsumura, J. Phys. Soc. Jpn. **82**, 054709 (2013).

[31] D. D. Khalyavin, D. T. Adroja, A. Bhattacharyya, A. D. Hillier, P. Manuel, A. M. Strydom, J. Kawabata, and T. Takabatake, arXiv: 1311.2904v1.

[32] H. Miwa: Prog. Theor. Phys. **28**, 208 (1962).

[33] T. Ishiga, R. Yoshida, H. Okazaki, K. Tsubota, M. Sunagawa, K. Uenaka, K. Okada, H. Kumigashira, M. Oshima, K. Yutani, Y. Muro, T. Takabatake, T. Wakita, Y. Muraoka, and T. Yokoya, unpublished.

[34] B. Cornut and B. Coqblin: Phys. Rev. B **5**, 4541 (1972).

[35] K. Umeo, T. Ohsuka, Y. Muro, J. Kajino, and T. Takabatake, J. Phys. Soc. Jpn. **80**, 064709 (2011).

[36] T. Susaki, Y. Takeda, M. Arita, K. Mamiya, A. Fujimori, K. Shimada, H. Namatame, M. Taniguchi, N. Shimizu, F. Iga, and T. Takabatake, Phys. Rev. Lett. **82**, 992 (1999).

[37] T. Ekino, T. Takabatake, H. Tanaka, and H. Fujii, Phys. Rev. Lett. **75**, 4262 (1995).

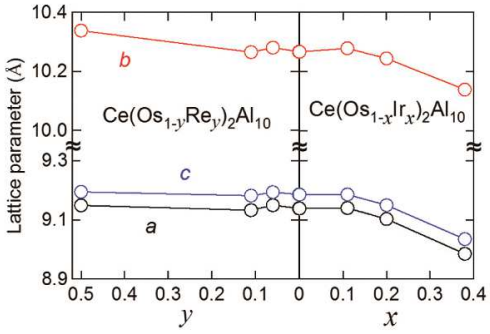

FIG. 1. Lattice parameters of polycrystalline samples of $Ce(Os_{1-x}Ir_x)_2Al_{10}$ and $Ce(Os_{1-y}Re_y)_2Al_{10}$, which crystalize in the orthorhombic $YbFe_2Al_{10}$-type structure.

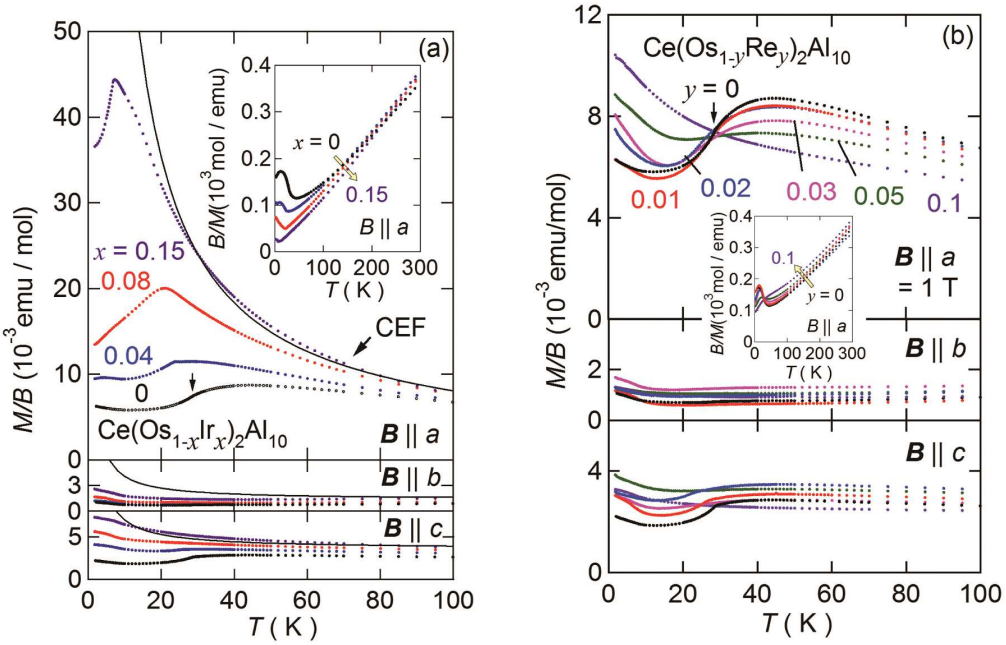

FIG. 2. Temperature dependence of magnetic susceptibility for single crystals of (a) $Ce(Os_{1-x}Ir_x)_2Al_{10}$ and (b) $Ce(Os_{1-y}Re_y)_2Al_{10}$ along the three principal axes.

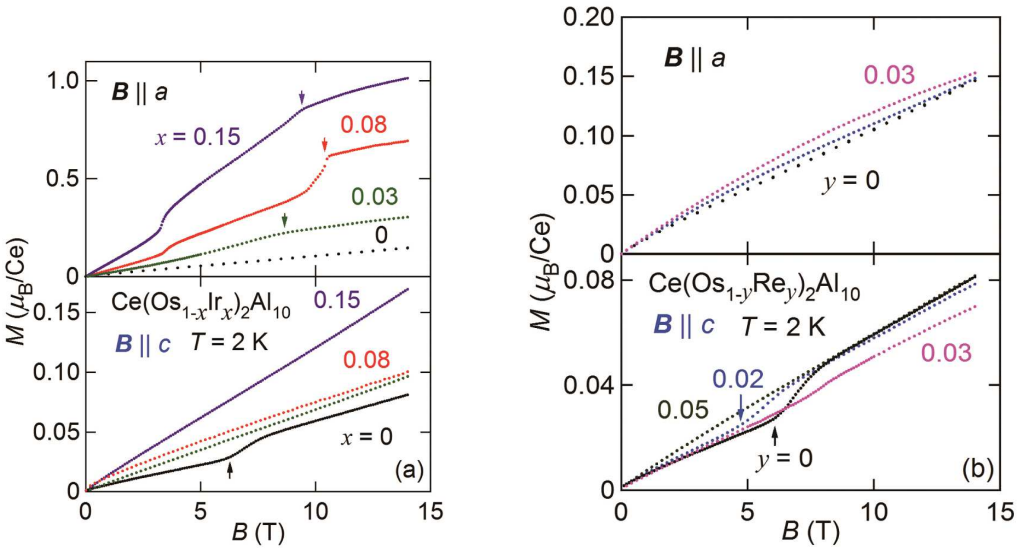

FIG. 3. Isothermal magnetization $M(B \parallel a)$ and $M(B \parallel c)$ at 2 K for (a) $Ce(Os_{1-x}Ir_x)_2Al_{10}$ and (b) $Ce(Os_{1-y}Re_y)_2Al_{10}$.

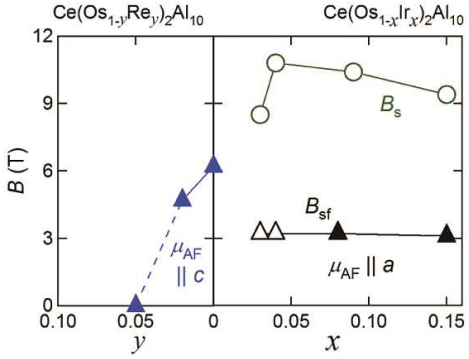

FIG. 4. Variations of the spin-flop field B_{sf} and the field toward saturation B_s in the isothermal magnetization curve $M(B)$ as a function of x and y in $Ce(Os_{1-x}Ir_x)_2Al_{10}$ and $Ce(Os_{1-y}Re_y)_2Al_{10}$.

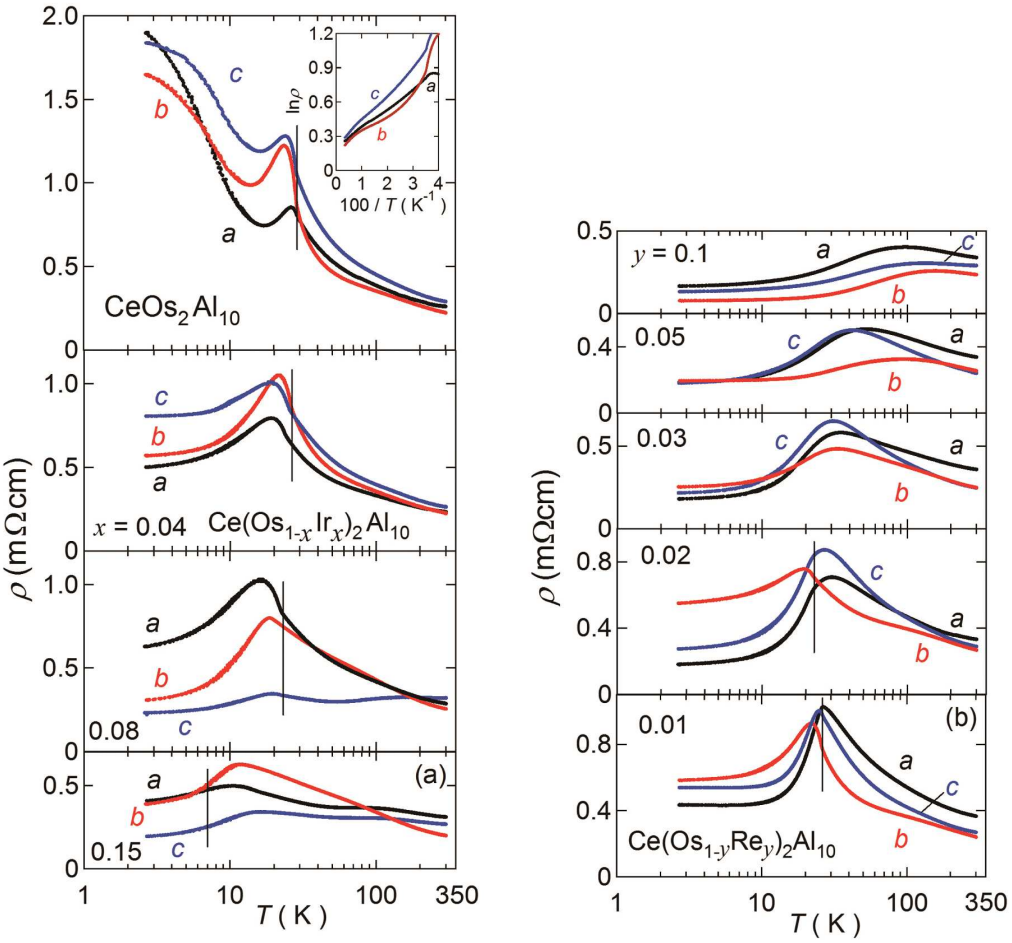

FIG. 5. Temperature dependence of electrical resistivity for single crystals of (a) $Ce(Os_{1-x}Ir_x)_2Al_{10}$ and (b) $Ce(Os_{1-y}Re_y)_2Al_{10}$ along the three principal axes.

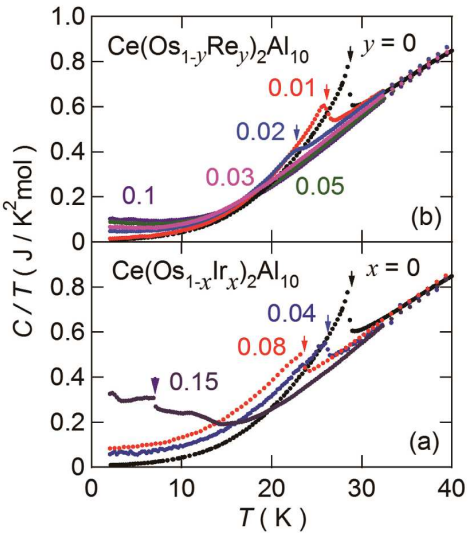

FIG. 6. Temperature dependence of specific heat divided by temperature C/T for (a) $Ce(Os_{1-x}Ir_x)_2Al_{10}$ and (b) $Ce(Os_{1-y}Re_y)_2Al_{10}$.

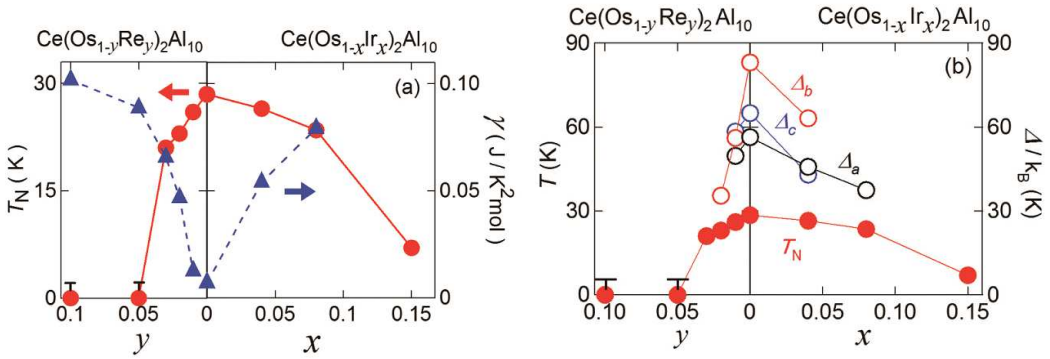

FIG. 7. Variations of (a) the Néel temperature T_N and the γ value of the specific heat and (b) T_N and the thermal activation energy Δ in the resistivity as a function of x and y in $Ce(Os_{1-x}Ir_x)_2Al_{10}$ and $Ce(Os_{1-y}Re_y)_2Al_{10}$.